Crystal characterization and optical spectroscopy of Ti^{3+}-doped $CaGdAlO_4$ crystals

Nobuhiro Kodama
Department of Chemistry, Faculty of Education, Akita University, Akita 010, Japan

Mitsuo Yamaga
Department of Electronics, Faculty of Engineering, Gifu University, Gifu 501-11, Japan

(Received 8 September 1997)

$CaGdAlO_4$ crystals doped with Ti ions were grown using the Czochralski technique in a reducing atmosphere in order to convert the valence of Ti to trivalence. The fluorescence of the $^2E \rightarrow {}^2T_2$ transition of Ti^{3+} in the crystals shows a broad band with a peak at 535 nm excited with the light of 410 nm in the optical absorption band at room temperature because of a strong electron-phonon coupling of the ^2E excited state. The Ti^{3+} fluorescence is influenced in intensity by O^{2-} vacancies at the ligands of the Ti^{3+} octahedra along the c axis, which are easily produced in a reducing atmosphere. The x-ray crystal analyses and the polarization of the optical absorption and fluorescence spectra deduce the energy levels and wave functions of the ground and excited states of Ti^{3+} in $CaGdAlO_4$. The peak energy of the fluorescence band shifts to higher energy as increasing excitation energy in the absorption band. The linear dependence of the fluorescence-peak energy on the excitation energy shows that the fluorescence is inhomogeneously broadened by a random distribution of Ca^{2+} and Gd^{3+} ions in the disordered lattice. [S0163-1829(98)01602-6]

I. INTRODUCTION

Ti^{3+}-doped crystals have attracted considerable interest in view of their potentials as tunable solid-state laser materials. Up to now, both the cw and pulsed laser oscillations have been performed for Ti^{3+}:Al_2O_3 in the near-infrared region of 0.7–1.1 μm,[1] and the pulsed laser action of Ti^{3+}:$BeAl_2O_4$ (Ref. 2) and Ti^{3+}:$Y_3Al_5O_{12}$ (YAG) (Ref. 3) have been successful. However, laser actions using these Ti^{3+}-doped crystals cannot be achieved in a visible region. In order to achieve a laser action in blue and green regions, new host crystals doped with Ti^{3+} are required to have a strong octahedral crystal field.

In a previous paper,[4] the authors have reported that the crystal-field splitting of Ti^{3+} in $CaGdAlO_4$ (Ti:CGA) is larger than those in Al_2O_3, YAG, and $YAlO_3$ (Ref. 5) and that the fluorescence wavelength of Ti^{3+} in this crystal is shifted into a green region. Although we tried to achieve a laser action of Ti:CGA under cw or pulsed laser pumping, it was not successful because of the weak stimulated emission. The intensity of the Ti^{3+} fluorescence in CGA was strongly dependent on the crystal-growth condition.

The electronic properties of Ti^{3+} in $CaYAlO_4$ (CYA) of the same crystal families as CGA were examined using optical and electron spin resonance (ESR) measurements.[6] The fluorescence could hardly be observed because of the large nonradiative decay due to local phonons created around O^{2-} vacancies near to Ti^{3+} ions. The O^{2-} vacancies may be produced by low O_2 partial pressure in a crystal growth under a reducing atmosphere, which is required to convert Ti^{4+} to Ti^{3+}. Since the creation of the O^{2-} vacancies causes deviation from stoichiometry of the crystals, the fluorescence intensity is expected to be related to nonstoichiometry of the crystals. In order to examine the relationship between Ti^{3+}-fluorescence properties and host crystal compositions, various crystals with the formula Ti_p:$(Ca,Mg)_{1+x}(Gd,La)_{1+y}Al_{1+z}O_{4-\delta}$ [$\delta = -\{3(p+y+z)+2x\}/2$] have been grown. This paper discusses the energy levels and wave functions of the ground and excited states of Ti^{3+} in CGA in terms of the x-ray structure analysis and the optical polarization, and the inhomogeneous broadening of the fluorescence spectra caused by substitutional disorder of the Ca^{2+}/Gd^{3+} sites in the Ti:CGA crystal lattice.

II. EXPERIMENTAL

The $CaGdAlO_4$ (CGA) crystal with the K_2NiF_4 structure is tetragonal with the space group $I4/mmm$, containing two formula units in a unit cell as shown in Fig. 1. The CGA crystal is isomorphous with $CaYAlO_4$ (CYA) and $SrLaAlO_4$ (SLA), of which the structures were refined by Shannon *et al.*[7] Impurities Ti^{3+} substitute for Al^{3+} ions. CGA single crystals doped with Ti^{3+} ions were grown by the Czochralski method from stoichiometric or nonstoichiometric melts of Ti_p:$(Ca,Mg)_{1+x}(Gd,La)_{1+y}Al_{1+z}O_{4-\delta}$ [$\delta = -\{3(p+y+z)+2x\}/2$] under a reducing atmosphere [$Ar+H_2(0.4\%)$]. The crystal growth was made using a pulling apparatus. The chemicals $CaCO_3$ and MgO with $4N$ purity and Gd_2O_3, La_2O_3, Al_2O_3, and TiO_2 with $5N$ purity were used as the starting materials. Mixed powders of appropriate mole ratios in a rubber bag were pressed at 1500 Kg/cm^2 under a hydrostatic press. The pressed samples were melted by inductive heating at 1953–2093 K in an Ir crucible with diameter of 46 mm. After soaking for several hours, the melts were held at appropriate seeding temperatures. The Ti:CGA crystals were grown along the [100] axis at a pulling rate of 0.4 mm/h and a crystal rotation rate of 10 rpm.

The compositions of the as-grown crystals were determined by the inductively coupled plasma (ICP) emission analysis. The relative errors of the analyses are in a few percent. The crystal structures were refined by the least-squares method using the single-crystal x-ray-diffraction data measured by Sawada and Kodama.[8] The resulting boules were cut and polished into samples with approximate

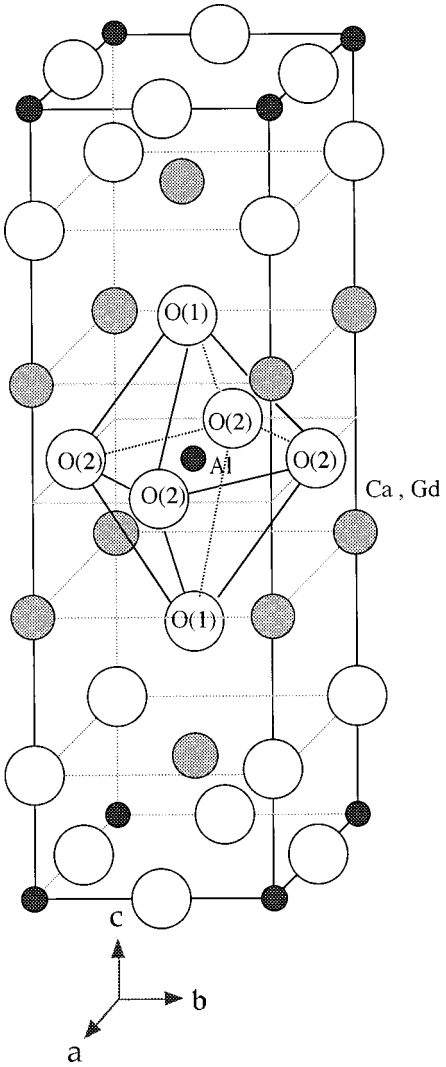

FIG. 1. Crystal structure of $CaGdAlO_4$. Small shaded circle, large shaded circle, and open circle denote Al^{3+}, Ca^{2+}, or Gd^{3+} and O^{2-} ions, respectively.

dimensions $5\times5\times5$ mm^3 for optical measurements, the cut faces being normal to [100], [010], and [001] directions.

The optical absorption spectra were measured at room temperature using an Hitachi A-4000 double-beam spectrophotometer. The fluorescence and excitation spectra were measured using an Hitachi F-4500 fluorescence spectrophotometer at room temperature and calibrated using Rhodamine-B solution in the range 200–600 nm. The polarizations of the absorption and fluorescence spectra were measured using a Glan-Taylor prism.

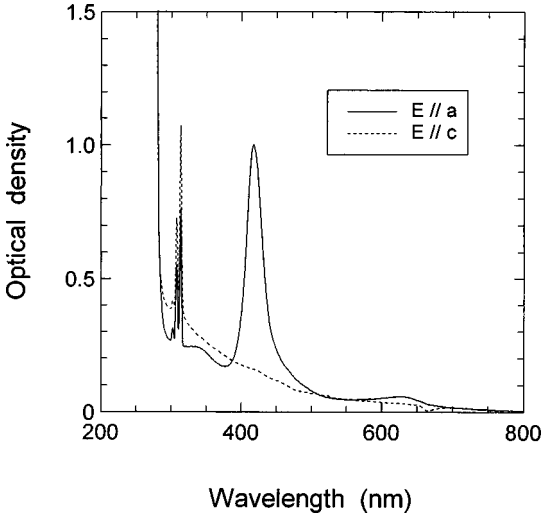

FIG. 2. The polarized absorption spectra of Ti:CGA-1 measured at room temperature. The E vectors of the light are parallel to the a and c axes.

III. EXPERIMENTAL RESULTS

A. Crystal compositions

The compositional formulas of the as-grown crystals are expressed by $Ti_p:(Ca,Mg)_{1+x}(Gd,La)_{1+y}Al_{1+z}O_{4-\delta}$, where the O^{2-} deficiency δ is equal to $-\{3(p+y+z)+2x\}/2$ on the basis of crystal neutrality. The crystal compositions are listed in Table I, together with the starting compositions. They are not coincident with each other. The values of δ in Table I increase with decreases of ratios of Ca^{2+} and/or Al^{3+} to Gd^{3+} in the starting compositions.

B. Optical absorption spectra

The optical absorption spectra of the five crystals with different chemical compositions in Table I were measured at room temperature. Figure 2 shows the polarized absorption spectra observed for Ti:CGA-1. The absorption spectra consist of sharp lines (308 nm, 314 nm) due to Gd^{3+} ions,[9] and two broad bands with peaks at 410 and 620 nm. The absorption band with its peak at 410 nm is polarized parallel to the a axis more strongly than to the c axis. Annealing the as-grown crystals in a reducing atmosphere enhances the 410-

TABLE I. Crystal compositions of $Ti_p:(Ca,Mg)_{1+x}(Gd,La)_{1+y}Al_{1+z}O_{4-\delta}$ determined by the ICP emission analysis in comparison with starting composition ratios. The O^{2-} deficiencies are calculated on the basis of the restriction of crystal neutrality $\delta=-\{3(p+y+z)+2x\}/2$.

	Starting composition ratio							
Abbreviation	Ca:	Mg:	Gd:	La:	Al:	Ti	Crystal composition	O^{2-} deficiency δ
Ti:CGA−1	1.10		0.90		0.99	0.02	$Ti_{0.01}:Ca_{1.00}Gd_{1.00}Al_{0.98}O_{3.98}$	0.02
Ti:CMGA	0.99	0.02	0.99		0.98	0.02	$Ti_{0.01}:Ca_{0.96}Mg_{0.02}Gd_{0.99}Al_{0.99}O_{3.96}$	0.04
Ti:CGLA	1.00		0.90	0.10	0.98	0.02	$Ti_{0.01}:Ca_{1.00}Gd_{0.95}La_{0.05}Al_{0.96}O_{3.95}$	0.05
Ti:CGA−2	1.00		1.00		0.98	0.02	$T_{0.01}:Ca_{1.02}Gd_{0.98}Al_{0.97}O_{3.94}$	0.06
Ti:CGA−3	0.80		1.20		0.98	0.02	$Ti_{0.004}:Ca_{0.99}Gd_{1.01}Al_{0.94}O_{3.92}$	0.08

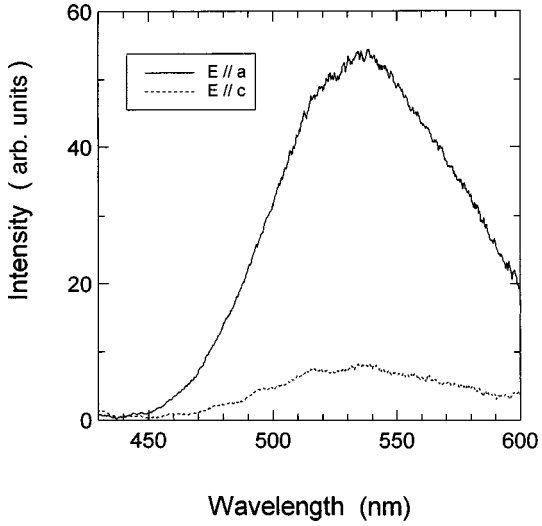

FIG. 3. The polarized fluorescence spectra excited at 410 nm for Ti:CGA-1 and measured at room temperature. The E vectors of the fluorescence are parallel to the a and c axes. The intensities of the spectra are calibrated in the range 400–600 nm.

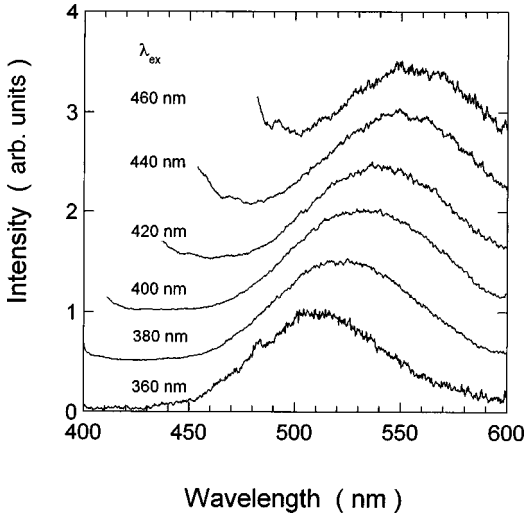

FIG. 4. The fluorescence spectra of Ti^{3+} in Ti:CGA-1 with different excitation wavelengths measured at room temperature. The spectra are normalized at the peaks and calibrated in the range 400–600 nm.

nm band and produces newly a 550-nm band. The 550-nm absorption band is also strongly polarized parallel to the a axis and the component polarized parallel to the c axis is negligibly weak. The absorption spectra for the other four crystals, Ti:CMGA, Ti:CGLA, Ti:CGA-2, and Ti:CGA-3 are almost the same as that for Ti:CGA-1, the relative intensities of the two bands being somewhat different.

The polarizations of these absorption spectra in Ti:CGA are the same as those in Ti:CYA.[6] The origins of the 620-nm band in the as-grown crystal and the 550-nm band in the annealing sample are not yet clear. Excitation in the 550- and 620-nm absorption bands does not produce any fluorescence in the range 600–900 nm at room temperature. Here, we focus on the 410-nm absorption band.

C. Fluorescence and excitation spectra

Excitation at wavelengths in the 410-nm absorption band produces a green broadband fluorescence with a peak around 535 nm at room temperature. Figure 3 shows the polarized fluorescence spectra for Ti:CGA-1 excited at 410 nm. The intensity of the fluorescence polarized parallel to the a axis is much stronger than that polarized parallel to the c axis. Figure 4 shows the fluorescence spectra of Ti:CGA-1 excited at different wavelengths in the 410-nm absorption band. The spectra are normalized at the peak and calibrated in the range 400–600 nm. As shown in Fig. 4, the peaks in the fluorescence spectra shift to longer wavelengths with increasing excitation wavelengths. The dependence of the peak energy of the fluorescence on the excitation energy for Ti:CGA-1 is shown in Fig. 5. The peak energy varies linearly with the excitation energy. The gradient of the straight line calculated using the method of least squares is about 0.24.

The excitation spectra of the fluorescence detected at various fixed wavelengths for Ti:CGA-1 are shown in Fig. 6. The excitation spectra for the fluorescence at the fixed wavelengths of less than 480 nm show a single peak, while those at the wavelengths of more than 500 nm have a dip around 418 nm. The dip appears clearly when the peak of the excitation spectrum shifts to longer wavelengths. Such dips are observed for all five samples. The excitation spectra decrease in intensity and the dips deepen with an increase of the O^{2-} deficiency δ in a series of the crystals in Table I. The dip is attributed to the reabsorption of nonradiative centers, such as a complex of Ti^{4+} and O^{2-} vacancy,[6] of which the absorption overlaps in the 410 nm band. The excitation spectrum without the dip is very similar to the absorption spectrum in Fig. 2. Taking into account that the absorption, fluorescence, and excitation spectra are fairly broad, and that the radiative center is stable up to room temperature, the absorption and fluorescence spectra are assigned to be due to the $^2T_2 \leftarrow {}^2E$ transitions with different electron-phonon coupling of the $^2T_2$ ground state and ^2E excited state of Ti^{3+} in CGA.

The fluorescence bands with the peak at 535 nm were observed for the other four crystals Ti:CMGA, Ti:CGLA, Ti:CGA-2, and Ti:CGA-3 under the same experimental conditions. Figure 7 shows the integrated intensity of the

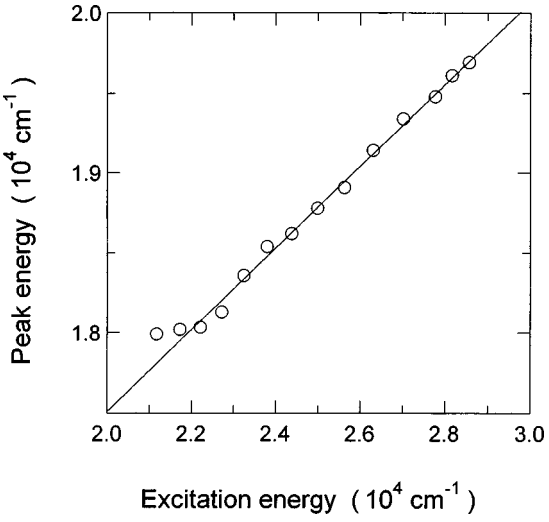

FIG. 5. The dependence of the peak energy of the fluorescence on the excitation energy for Ti:CGA-1.

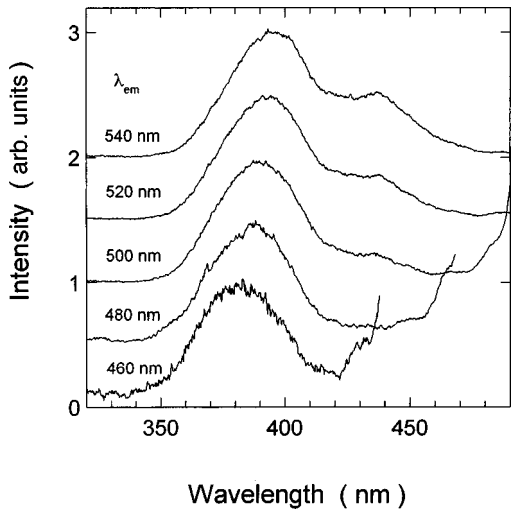

FIG. 6. The excitation spectra of the fluorescence detected at different fixed wavelengths for Ti:CGA-1 at room temperature. The spectra are normalized at the peaks and calibrated in the range 300–500 nm.

Ti^{3+}-fluorescence band as a function of the O^{2-} deficiency δ. The intensity rapidly decreases as δ increases. The Ti:CGA-1 crystal shows the maximum intensity and the fluorescence of the Ti:CGA-2 is reduced to about one order of magnitude in intensity compared with that of Ti:CGA-1. Further, the fluorescence intensity for Ti:CGA-3 with the largest O^{2-} deficiency of $\delta=0.08$ was negligibly small. These results are in agreement with those reported in the previous paper,[6] local phonons around the O^{2-} vacancy nearby the Ti^{3+} ion in CYA enhancing the nonradiative decay rate from the ^2E excited to the $^2T_2$ ground state of the Ti^{3+} ion.

IV. DISCUSSION

A. Relationship between Ti^{3+} octahedral structures and optical spectra

Ca^{2+} and Gd^{3+} ions in the CGA crystal are distributed at random on their common lattice sites with ninefold coordination, keeping the composition ratio of 1:1. Ti^{3+} ions substitute for Al^{3+} ions that form TO_6 (T=Al or Ti) octahedra in a unit cell. There are two kinds of O^{2-} ligand ions of the octahedron TO_6 with different symmetries, being denoted by O(1) and O(2) as shown in Fig. 1. CG (=Ca or Gd) and O(1) ions occupy the special positions of the site symmetry $4mm$, $(0,0,\pm z;\ \frac{1}{2},\ \frac{1}{2},\ \frac{1}{2}\pm z)$, T (=Al or Ti) ions occupy the special positions of $4/mmm$, $(0,0,0;\ \frac{1}{2},\ \frac{1}{2},\ \frac{1}{2})$, and O(2) ions occupy the special positions of mmm, $(0,\ \frac{1}{2},\ 0;\ \frac{1}{2},\ 0,0)$.

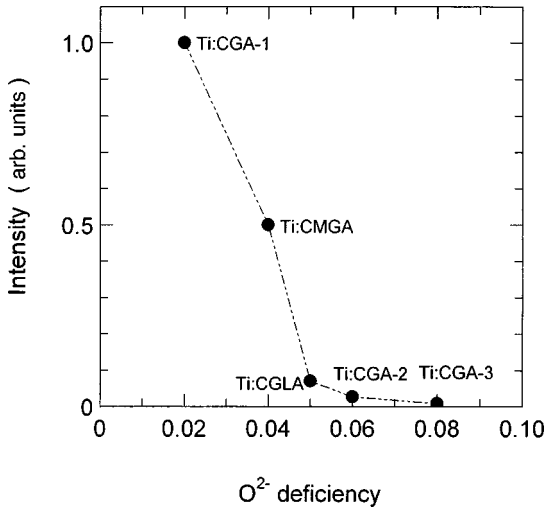

FIG. 7. Relationship between the integrated intensity of the Ti^{3+} fluorescence excited at 390 nm and the O^{2-} deficiency δ, in the crystals in Table I.

TABLE II. Atomic parameters and interatomic distances for Ti:CGA−1 and Ti:CGA−3. CG denotes Ca or Gd. T denotes Al or Ti. O(1) and O(2) are O^{2-} ions on c axis and in ab plane, respectively. z is a positional parameter. P stands for the site occupancy of the relevant ion. U_{11}, U_{22} and U_{33} stand for the mean-square displacements from the equilibrium positions of the ions.

		Ti:CGA−1	Ti:CGA−3
Atomic parameters			
CG	z	0.35857(1)	0.35863(1)
	P	0.97(1)	0.95(1)
	$U_{11}(=U_{22})$	0.00587(2)	0.00538(3)
	U_{33}	0.00491(3)	0.00465(4)
T	P	0.99(1)	0.98(1)
	$U_{11}(=U_{22})$	0.0033(1)	0.0034(2)
	U_{33}	0.0100(3)	0.0100(4)
O(1)	z	0.1677(1)	0.1677(2)
	P	0.96(1)	0.93(1)
	$U_{11}(=U_{22})$	0.0155(4)	0.0152(5)
	U_{33}	0.0060(3)	0.0055(4)
O(2)	P	1	1
	U_{11}	0.0033(2)	0.0032(3)
	U_{22}	0.0069(3)	0.0071(4)
	U_{33}	0.0103(3)	0.0103(5)
Interatomic distances (Å)			
CG-CG		3.3912(2)	3.3890(2)
T-O(1)		2.010(1)	2.010(2)
T-O(2)		1.8309(1)	1.8303(2)

The crystal structures of Ti:CGA-1 with the smallest O^{2-} deficiency and Ti:CGA-3 with the largest one have been refined using the single-crystal x-ray-diffraction data[8] and the least-squares method. The atomic parameters of the K_2NiF_4 structure are used as starting parameters. The atomic parameters are refined by minimizing the sum of the difference between the observed and calculated structure factors of crystals assuming crystal neutrality. The refined atomic parameters, positional parameters z, population parameters P, and anisotropic thermal parameters U_{11}, U_{22}, and U_{33} are summarized in Table II. P represents site occupancy of ions. U_{11}, U_{22}, and U_{33} are mean-square displacements of ions from the equilibrium positions along the directions parallel to the a, b, and c axes, respectively. Then, $\sqrt{U_{ii}}$ $(i=1,2,3)$ represents time mean displacements of ions. The unity of P means the stoichiometric composition. The result that the values of P for CG, T, and O(1) are less than 1 indicates the deviation from the stoichiometric compositions. The interatomic distances calculated using the atomic parameters are also summarized in Table II. The chemical compositions of Ti:CGA-1 and Ti:CGA-3 are given as the forms

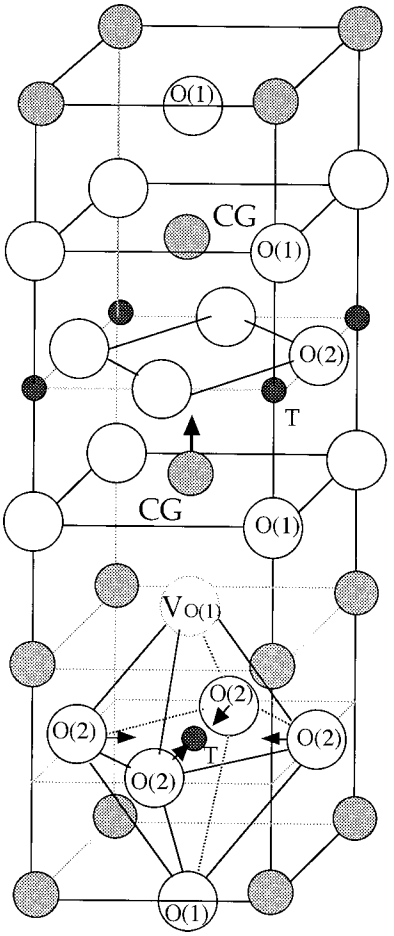

FIG. 8. The crystal structure including an octahedron accompanied with an O^{2-} vacancy [$V_{O(1)}$] at the O(1) site along the c axis, and the displacement directions (→) of the CG (=Ca or Gd) and O(2) ions.

of $Ca_{0.97(1)}Gd_{0.97(1)}Al_{0.98(1)}Ti_{0.01(1)}O(1)_{1.92(3)}O(2)_2$ and $Ca_{0.95(1)}Gd_{0.95(1)}Al_{0.97(1)}Ti_{0.01(1)}O(1)_{1.86(4)}O(2)_2$ assuming that the Ca/Gd ratio is equal to 1. They are in agreement with those in Table I obtained by the ICP emission analyses with relative errors of about 5%.

The compositions suggest that the O^{2-} vacancy is more preferentially created at the O(1) site than at the O(2) site, that is, that the T-O(1) bond is more easily broken than the T-O(2) bond in the crystal growth. This is confirmed by the fact that the interatomic distances of T-O(1), which correspond inversely to the bond strength, is longer than that of T-O(2) in both of Ti:CGA-1 and Ti:CGA-3. There is a little difference in the O(1) populations P of Ti:CGA-1 and Ti:CGA-3. It may be associated with the concentration of O^{2-} vacancies in these crystals. In order to confirm this relation, we consider the effects of O^{2-} vacancies on the local crystal structure. The O^{2-} vacancy reduces the coordination number of CG ions from nine to eight, resulting in the decrease of the negative charge distribution. The rearrangement of ions surrounding the vacancy occurs so as to compensate such a change of the distribution. The CG ion is displaced along the positive c axis and the four O(2) ions are displaced towards the center of the T ion as shown in Fig. 8. This expectation is in agreement with the result that the CG-CG interatomic distance and T-O(2) bond length in

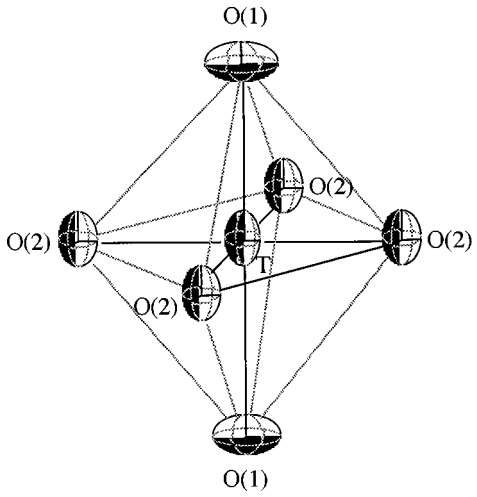

FIG. 9. Thermal vibration ellipsoids of T (=Al or Ti) and O^{2-} ions in the TO_6 octahedron for Ti:CGA-1.

Ti:CGA-3 are shorter than those in Ti:CGA-1 in Table II. In consequence, the comparison of the O(1) population, T-O(2) bond length and CG-CG interatomic distance in both crystals deduces that the O^{2-} vacancy concentration on the O(1) sites in Ti:CGA-3 is higher than that in Ti:CGA-1.

Taking into account the above results, we consider the reason why the Ti^{3+}-fluorescence intensity decreases as a series of Ti:CGA-1, Ti:CMGA, Ti:CGLA, Ti:CGA-2, and Ti:CGA-3. Quenching the fluorescence is ascribed to nonradiative decay with multiphonon process. The phonons are strongly associated with the local phonons around Ti^{3+} ions in the crystal. The x-ray structure analyses give the result that O^{2-} vacancies on the O(1) sites increase as the above crystal series. Local phonons created around O^{2-} vacancy nearby the Ti^{3+} ion enhance nonradiative decay rate from the ^2E excited to $^2T_2$ ground states. Therefore, the decrease of the fluorescence is due to the increase of the nonradiative Ti^{3+} centers accompanied by the O^{2-} vacancies.

Next, consider thermal parameters U_{11}, U_{22}, and U_{33}, being associated with lattice vibration modes of the octahedron. Their values are summarized in Table II. There is no significant difference between Ti:CGA-1 and Ti:CGA-3. Figure 9 shows the thermal vibration ellipsoids of each ion in the TO_6 octahedron in Ti:CGA-1, which represent the relative magnitude of the time mean displacements of ions from the equilibrium positions. The displacements of the O(1) ions are larger in the ab plane than along the c axis, whereas those of the O(2) ions and the central T ion are reverse. This result suggests that the x and/or y components of the T_{2g} even-parity phonon mode and the z component of the T_{1u} and/or T_{2u} odd-parity phonon modes are dominantly created in the TO_6 octahedron, where the notations x, y, and z are corresponding to the a, b, and c axes, respectively.

The x-ray structure analyses in Table II conclude that the Ti^{3+} octahedron is elongate along the c axis and shows orthorhombic symmetry. This result is consistent with the identification of Ti^{3+} in CYA according to the ESR results.[6] The energy levels of the ground and excited state of Ti^{3+} in orthorhombic symmetry are expected to be ($|yz\rangle$, $|zx\rangle$, $|xy\rangle$) and ($|2z^2-x^2-y^2\rangle$, $|x^2-y^2\rangle$) in order of increasing energy as shown in Fig. 10. The T_{1u} and T_{2u} odd-parity phonon

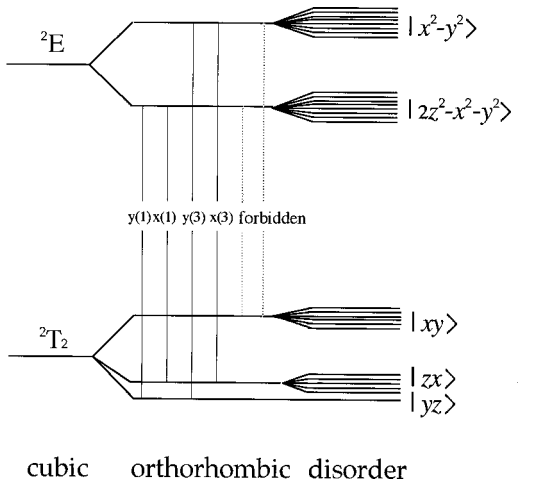

FIG. 10. Energy levels and eigenfunctions of the ground and excited states of Ti^{3+} in orthorhombic symmetry including a disorder effect. Polarization and relative intensities of optical transitions induced by the z component of T_{1u}/T_{2u} odd-parity phonons.

modes estimated from the thermal parameters are important in allowing electric dipole radiative transitions between the excited and ground states of Ti^{3+}. Such odd-parity phonon modes determine the polarizations of the optical absorption and fluorescence transitions. The selection rule for the intermanifold transitions of Ti^{3+} ions in sites with octahedral, tetragonal, trigonal, and orthorhombic symmetry have been discussed by Yamaga and co-workers,[10] using a model in which odd-parity distortions or phonon modes mix odd-parity wave functions from neighboring ligand ions into the even-parity $3d$ orbitals. They have calculated the transition probabilities between the ^2E excited state and $^2T_2$ ground state induced by T_{1u} and T_{2u} modes. Figure 10 shows the polarization of the transitions of Ti^{3+} in orthorhombic symmetry, induced by the z components of T_{1u} and T_{2u}. The transitions between the $|yz\rangle$, $|zx\rangle$ ground states and the $|2z^2-x^2-y^2\rangle$, $|x^2-y^2\rangle$ excited states are allowed, whereas those between the $|xy\rangle$ ground state and the $|2z^2-x^2-y^2\rangle$, $|x^2-y^2\rangle$ excited states are still forbidden. The electric dipole transitions are only the x and y components. This result agrees with the polarization of the absorption spectrum (Fig. 2) and the fluorescence spectrum (Fig. 3).

B. Inhomogeneous broadening of the Ti^{3+} fluorescence

Ti^{3+} ions preferentially occupy Al^{3+} sites in the CGA crystals, which are octahedral coordinated to six nearest-neighbor oxygen ligand ions with eight Ca^{2+}/Gd^{3+} second-neighbor ions. The Ca^{2+} and Gd^{3+} ions randomly occupy their common lattice sites. In addition, O^{2-} vacancies distribute on O(1) sites in the vicinity of the Ti^{3+} octahedra and/or in the Ti^{3+} octahedra. The substitutional disorder of the Ca^{2+} and Gd^{3+} ions and the distribution of the O^{2-} vacancies in the lattice produce a distribution of the crystal field of the Ti^{3+} ions, which cause the inhomogeneous broadening of the optical spectra.

In previous papers,[11–13] the authors reported the inhomogeneous broadening of optical spectra in V^{4+}, Cr^{3+}, and Ce^{3+} in CYA crystals, which have distributions of the crystal fields caused by substitutional disorder of the Ca^{2+}/Y^{3+} sites in the crystal lattice. The linear dependence of the peak energy of the fluorescence on the excitation energy for Ti:CGA (Fig. 5) is the same as has been observed for V^{4+}:CYA (Ref. 11) and Ce^{3+}: CYA.[13] This result suggests that the Ti^{3+} fluorescence is also inhomogeneously broadened as a consequence of the random distribution of Ca^{2+} and Gd^{3+} ions in different unit cells in CGA, including the distribution of O^{2-} vacancy in the vicinity of Ti^{3+} ion. Figure 10 shows the schematic energy levels and eigenfunctions of the ground and excited states of Ti^{3+} in orthorhombic symmetry including disorder effect in CGA.

We have extended the convolution method for V^{4+}:CYA,[11] Ce^{3+}:CYA (Ref. 13), and Cr^{3+}:glasses[14,15] to the Ti^{3+} fluorescence in CGA crystals. The slope of the fluorescence peak energy against the excitation energy is calculated to be $\gamma^2/(\Gamma^2+\gamma^2)$, where Γ is the linewidth of the intrinsic absorption and fluorescence line shapes and γ is the width of the distribution of the lowest ^2E excited energy level created by the disorder, assuming that their functions are Gaussians. The slope is obtained to be 0.24 from the experimental data of Fig. 5. It is very close to that (0.25) observed in V^{4+}:CYA. The linewidth of the intrinsic fluorescence and the width of the distribution function are separately estimated to be $\Gamma=1073\ cm^{-1}$ and $\gamma=603\ cm^{-1}$ using the calculated slope $\gamma^2/(\Gamma^2+\gamma^2)$ and the observed width ($1195\ cm^{-1}$) of the fluorescence band in Fig. 4. The inhomogeneous broadening of the observed fluorescence spectrum enlarges the linewidth with an amount of 11%, compared with the intrinsic linewidth.

V. CONCLUSION

Several Ti-doped $CaGdAlO_4$ single crystals with different starting compositions were grown in a reducing atmosphere by the Czochralski method. The crystals with less O^{2-} vacancies show stronger broad fluorescence band of Ti^{3+} with the peak at 535 nm excited at 410 nm at room temperature. The results of the x-ray crystal-structure analyses have suggested that radiative Ti^{3+} centers occupy perfect octahedra, whereas the nonradiative Ti^{3+} centers are accompanied by the vacancy of the O^{2-} ligand ion along the c axis in the Ti^{3+} octahedron. Nonradiative decay from the ^2E excited to $^2T_2$ ground states of Ti^{3+} occurs probably through local phonon modes coupled with the O^{2-} ligand vacancy. The x-ray analyses, also, conclude that the Ti^{3+} octahedron is elongated along the c axis and that the thermal vibration modes T_{1u} and T_{2u} exist dominantly in the octahedron. These results can explain the observed polarization of the absorption and fluorescence spectra of Ti^{3+} in CGA. The peak wavelength of the Ti^{3+}-fluorescence band shifts to longer wavelength with increasing excitation wavelength in the 410-nm absorption band. This peak shift gives evidence that the fluorescence is inhomogeneously broadened by the random distribution of the Ca^{2+}/Gd^{3+} sites in the disordered lattice.

ACKNOWLEDGMENTS

The work has been supported by a Grant-in-Aid for Scientific Research on Fundamental Research (No. 07650049) from the Ministry of Education, Science and Culture.

[1] P. Moulton, Opt. Photonics News **8**, 9 (1982).
[2] E. V. Pestryakov, V. I. Trunov, and A. I. Alimpiev, Sov. J. Quantum Electron. **17(5)**, 585 (1987).
[3] F. Bantien, P. Albers, and G. Huber, J. Lumin. **36**, 363 (1987).
[4] M. Yamaga, Y. Naitoh, and N. Kodama, in *Proceedings of the XII International Conference on Defects in Insulating Materials*, edited by O Lanert and J.-M. Spaeth (World Scientific, Singapore, 1993).
[5] T. Wegner and K. Petermann, Appl. Phys. B: Photophys. Laser Chem. **49**, 275 (1990).
[6] M. Yamaga, T. Yosida, Y. Naitoh, and N. Kodama, J. Phys.: Condens. Matter **6**, 4381 (1994).
[7] R. D. Shannon, R. A. Oswald, J. B. Parise, B. H. T. Chai, P. Byszewski, A. Pajaczkowska, and R. Sobolewski, J. Solid State Chem. **98**, 90 (1992).
[8] H. Sawada and N. Kodama (unpublished).
[9] G. H. Dieke and H. M. Crosswhite, Appl. Opt. **2**, 675 (1963).
[10] M. Yamaga, B. Henderson, and K. P. O. Donnell, Appl. Phys. B: Photophys. Laser Chem. **52**, 122 (1991).
[11] M. Yamaga, B. Henderson, T. Yosida, N. Kodama, and Y. Inoue, Phys. Rev. B **51**, 3438 (1995).
[12] M. Yamaga, P. I. Macfarlane, K. Holliday, B. Henderson, N. Kodama, and Y. Inoue, J. Phys.: Condens. Matter **8**, 3487 (1996).
[13] N. Kodama, B. Henderson, and M. Yamaga, J. Phys.: Condens. Matter **8**, 3505 (1996).
[14] M. Yamaga, B. Henderson, K. P. O'Donnell, and Y. Gao, Phys. Rev. B **44**, 4853 (1991).
[15] B. Henderson, M. Yamaga, Y. Gao, and K. P. O'Donnell, Phys. Rev. B **46**, 652 (1992).